

1 Daytime Passive Radiative Cooling by Ultra  
2 Emissive Bio-inspired Polymeric Surface

3 *S.Y. Jeong*<sup>1</sup>, *C.Y. Tso*<sup>1,\*</sup>, *Y.M. Wong*<sup>2</sup>, *C.Y.H. Chao*<sup>3</sup>, *B. Huang*<sup>2</sup>

4 <sup>1</sup> School of Energy and Environment, City University of Hong Kong, Tat Chee Avenue,  
5 Kowloon, Hong Kong, China

6 <sup>2</sup> Department of Mechanical and Aerospace Engineering, The Hong Kong University of Science  
7 and Technology (HKUST), Hong Kong, China

8 <sup>3</sup> Department of Mechanical Engineering, The University of Hong Kong, Hong Kong, China

9  
10 \* Corresponding Author Tel.: +852 3442 4623

11 E-mail address: [chiytso@cityu.edu.hk](mailto:chiytso@cityu.edu.hk)

12 Address: School of Energy and Environment, City University of Hong Kong, Tat Chee Avenue,  
13 Kowloon, Hong Kong, China

14

15

16 **Abstract**

17 Saharan silver ants can maintain their body temperature below ambient air due to unique triangular  
18 shaped hairs that enhance solar reflection and thermal emission through a transparent window that  
19 lies in the atmosphere. Applying this thermoregulatory prismatic structure to polydimethylsiloxane  
20 (PDMS), highly emissive in the 8-13  $\mu\text{m}$  spectrum, we present a geometrically modified polymer-  
21 based daytime passive radiative cooler. The selective thermal emitter was fabricated based on the  
22 optimized prismatic structure from Finite Difference Time Domain (FDTD) simulations. The  
23 average emissivity within the 8-13  $\mu\text{m}$  spectrum was enhanced to 0.98 by the gradient refractive  
24 index effect, while the average solar reflectivity in the visible and near-infrared spectrum was  
25 measured to be 0.95. The net radiative cooling power is estimated to reach 144  $\text{W}/\text{m}^2$ , exceeding  
26 records of previously reported radiative coolers. Last, in Hong Kong's hot and humid climate, a  
27 field test successfully demonstrated cooling by 6.2  $^{\circ}\text{C}$  below the temperature of ambient air  
28 corresponding to a net cooling power of 19.7  $\text{W}/\text{m}^2$  in a non-vacuum setup during the peak daytime  
29 with shading. This is the largest temperature reduction observed in a tropical region for daytime  
30 passive radiative cooling. Our work presents an alternative method to enhance passive thermal  
31 emission and may facilitate its world wide application in eco-friendly space cooling.

32

33 *Keywords: Gradient refractive index, Mie-scattering, Radiative cooling, Saharan silver ant,*  
34 *Selective emission, Thermal radiation*

35

36 **1. Introduction**

37 Daytime passive radiative cooling proposes a new eco-friendly strategy to solve the high energy  
38 demand for building space cooling. Conventional and widely used cooling methods require

39 external power sources or devices where high energy consumption is inevitable due to the  
40 necessities of everyday life. In contrast to the cooling methods utilizing resources and energy,  
41 passive radiative cooling solely focuses on the natural cooling strategies of near perfect solar  
42 energy reflection which lies in the visible (VIS) and near-infrared (NIR) spectrum, minimizing  
43 thermal absorption of incident solar irradiation. Furthermore, in the mid-infrared (MIR) spectrum  
44 (8-13  $\mu\text{m}$ ), the strong selective thermal radiation occurs from an object efficiently delivering  
45 thermal energy to the cold heat sink of outer space ( $\sim 3\text{ K}$ ) through the atmospheric transparency  
46 window where radiation absorption is very low in the 8-13  $\mu\text{m}$  spectrum. Nocturnal passive  
47 radiative cooling has been successfully conducted [1–10]; however, high cooling demands occur  
48 at peak hours during the daytime.

49

50 Recently, scientists and engineers have demonstrated a sky facing surface able to sustain its  
51 temperature below the temperature of ambient during daytime with a passive selective radiation  
52 strategy. A typical configuration of a daytime passive radiative cooler can be elaborated as two  
53 layered structures, including the top emissive layer and bottom reflective layer. Various materials  
54 and geometrical modifications in the top emissive layer were investigated to produce a cooling  
55 effect during daytime, such as photonic, plasmonic, biomimetic materials, etc. A photonic radiative  
56 cooler with a thermal emitter composed of seven repetitive layers of hafnium oxide ( $\text{HfO}_2$ ) and  
57 silicon dioxide ( $\text{SiO}_2$ ) and a solar reflector of silver (Ag), demonstrated a radiated power of 40  
58  $\text{W/m}^2$  and a daytime cooling performance of nearly  $5\text{ }^\circ\text{C}$  reduction below the temperature of  
59 ambient air [11]. This nanophotonic device which showed promising cooling performance in a dry  
60 region was tested in the sub-tropical climate of Hong Kong [12, 13]. A temperature reduction of  
61  $6\text{-}7\text{ }^\circ\text{C}$  was achieved under a clear night sky, but daytime cooling was not achieved in the humid

62 climate since the mid-infrared thermal emission is weakened by the huge amount of atmospheric  
63 water vapor. The nano-phonic approach requires precise and accurate fabrication, thus, the  
64 simplified radiative cooler was developed by deposition of silicon nitride ( $\text{Si}_3\text{N}_4$ ), and amorphous  
65 silicon (Si) on the top of a solar reflector of aluminum (Al) and in a vacuum condition, a strong  
66 daytime radiative cooling was achieved by 42 °C reduction below the ambient in the dry climate  
67 of California, USA [14]. A polymer based simplified passive cooler was proposed, designed with  
68 a polydimethylsiloxane (PDMS) polymer on top of the silver (Ag) sputtered glass ( $\text{SiO}_2$ ) wafer  
69 achieving a daytime cooling of 8.2 °C below the ambient relevant to a high radiative power of  
70 127  $\text{W}/\text{m}^2$  in low humidity California [15]. Photonic crystal structures theoretically and  
71 experimentally demonstrated selective thermal emission by surface plasmonic resonance [16–29].  
72 Different types of plasmonic radiative coolers were proposed including micropillar patterns on Al  
73 plate [30] and Ag deposited micro-patterned silicon (Si) wafers [31] demonstrating a numerically  
74 analyzed net cooling power of 100  $\text{W}/\text{m}^2$ . Generally, literatures report on lab scale radiative coolers  
75 with limited practical applications. Comprehensive reviews on a scaled-up glass-polymer hybrid  
76 radiative cooler by reel-to-reel processing has been carried out [32, 33]. Motivated by a polymeric  
77 radiative cooler with silicon carbide (SiC) and dispersed  $\text{SiO}_2$  micro-particles [34], a scalable  $\text{SiO}_2$   
78 micro-particle doped polymeric radiative cooler with the optimized particle size enhancing  
79 selective thermal emission in mid-infrared (MIR) emission was manufactured, recording a  
80 radiative power of 93  $\text{W}/\text{m}^2$  [33]. Daytime passive radiative coolers can be directly attached to  
81 fabrics [35, 36] and electronics [37, 38] for efficient cooling, or they can be integrated in a  
82 refrigeration cycle of HVAC systems in buildings as a condenser which saves energy consumed  
83 in space cooling due to its cooling performance without energy input [39-41].

84

85 Both organic and inorganic materials with strong emission property in the MIR wavelength  
86 spectrum (8-13  $\mu\text{m}$ ) were used as the base thermal emission substrate for passive radiative cooling  
87 [11–34]. In this study, for the first time, photonic approach on polymer was utilized to design a  
88 passive radiative cooler where geometry modification in polymer has been seldom considered to  
89 further enhance emission properties due to the challenge of controlling defects. However, polymer  
90 is a very attractive material due to its low cost, compatibility with various patterns, offering the  
91 required optical, electronic, and mechanical properties required [34, 42]. This work has been  
92 triggered by the Saharan silver ant shown in Fig. 1a that possesses two different passive thermal  
93 regulatory effects and successfully survives in extremely hot deserts. The Saharan silver ant has  
94 unique shaped hairs, in the form of triangular prisms, providing two thermoregulatory effects as  
95 shown in Fig. 1b that allows the ant to keep cool under the extremely strong sunlight of the Saharan  
96 desert [43–45]. The triangular shaped hair induces enhancement in total internal reflection within  
97 the solar spectrum (0.25 – 2.5  $\mu\text{m}$ ) resulting in high reflection of incident solar irradiance. The  
98 enhancement is realized by Mie scattering which takes place in situations where the size of the  
99 object is comparable to the wavelength of incident light, and for the ant, the scattering effect occurs  
100 at  $\sim 2 \mu\text{m}$  [46]. Furthermore, enhanced MIR emissivity of the hair facilitates heat dissipation of  
101 thermal energy accumulated in the ant's body which can easily escape through the transparent  
102 window. Shi et al. reported that due to its strong enhancement in solar reflection, the hair structure  
103 can be applied to develop a radiative cooler with a high reflective surface which does not require  
104 a metal reflector. However, the triangular prismatic structures were only able to achieve solar  
105 reflection of  $\sim 60\%$  which is far from the solar reflection requirement for radiative coolers (i.e.  $>$   
106  $95\%$ ) [44], thus, the application approach was newly established to enhance MIR thermal radiation  
107 of the daytime radiative cooling by utilizing gradual refractive index change effective in 8-13  $\mu\text{m}$ .

108

109     In this study, we propose a selective thermal emission device with application of the unique  
110 triangular prism shape of the Sahara silver ants' hair to perform enhanced radiative cooling  
111 performance. First, we investigated improvement in MIR thermal emission utilizing the micro-  
112 scale triangular prism structure compared to a conventional flat, multi-layered film and hair  
113 resembling a circular tube-structured cooler. The following study was conducted on the triangular  
114 structure for optimization to achieve the strongest thermal emission by controlling parameters such  
115 as the geometrical configurations and size. After computational optimization of the triangular  
116 structure, a passive radiative cooler employing the triangular prism array was then manufactured  
117 by a microfabrication process. To verify the result of the simulation study, the optical characteristic  
118 of the fabricated cooler was measured and a comparative study with the uniformly layered cooler  
119 was conducted. Based on the measured optical properties, its cooling performance was analyzed  
120 numerically with energy balance equations. Lastly, to test its practicality under the humid weather  
121 condition of Hong Kong with a low transparent atmospheric window, field investigations were  
122 carried out and the cooling performance was observed. This study indicates geometrical  
123 modification as a potential solution to improve selective thermal emission besides the selection of  
124 various materials, which can significantly improve the passive radiative cooling effect by scaling  
125 down, reducing materials required for manufacturing but enhancing the cooling power. This  
126 indicates that the biomimetic radiative cooler could be an attractive non-energy-consuming  
127 solution to reduce air conditioning costs for buildings in the near future.

128

## 129 **2. Material and methods**

### 130 **2.1. Design and optimization method**

131 In this study, we propose the bio-inspired passive daytime radiative cooler with a design of a top  
132 MIR emissive layer of PDMS and SiO<sub>2</sub> that strongly radiates in the 8-13 μm spectrum and a bottom  
133 solar reflective layer composed of Ag which can provide solar reflection above 95 %. Optimization  
134 was mainly focused on achieving the highest emissivity within the targeted MIR range (8-13 μm)  
135 due to the major contribution in net radiative cooling performance. PDMS and SiO<sub>2</sub> are already  
136 well known for being selectively emissive in 8-13 μm wavelength range due to a high value of  
137 imaginary permittivity [47]. Furthermore, the proposed cooler possesses an advantage of easy  
138 fabrication due to widely available SiO<sub>2</sub> substrate wafer (400-500 μm) and flexible material  
139 property of PDMS which can be easily shape to desired geometries on the surface by a nano-  
140 imprinting process. The great freedom to shape PDMS allows us to study the improvement of  
141 optical properties especially emissivity in different configurations. The geometrical structure on  
142 the surface of the PDMS emitter was optimized by utilizing FDTD simulations considering  
143 different geometries and sizes. After optimization, a comparison study regarding MIR emission  
144 between our optimized bio-inspired cooler and conventional flat surface cooler was performed.  
145 Prior to the fabrication and field experiment, FDTD optical computational analysis which directly  
146 solves Maxwell equations was utilized to achieve the highest net cooling power by optimizing  
147 geometrical structures of the PDMS emitter surface and the overall design of the cooler.

148

## 149 **2.2. Fabrication**

150 For the microfabrication of the optimized bio-inspired daytime radiative cooler, a mold with  
151 triangular prism patterns needs to be fabricated first which can later be used to print patterns on  
152 the PDMS layer. A 525 μm thick P-type 4” silicon wafer was used as the substrate for the triangular  
153 prism array mold. The silicon wafer first underwent pre-photolithography cleaning in Piranha

154 solution, mixture of 10:1 (v/v)  $\text{H}_2\text{SO}_4:\text{H}_2\text{O}_2$ , at 120 °C for 10 mins to remove organic residues and  
155 gross contaminants. Native oxide layer on the silicon wafer surface was removed by hydrofluoric  
156 acid solution, mixture of 1:50 (v/v)  $\text{HF}:\text{H}_2\text{O}$ , for 1 min. After the cleaning process, a thin silicone  
157 oxide layer of 60 nm was produced on the silicon wafer surface by thermal oxidation using a  
158 diffusion furnace at a temperature between 800 - 1200 °C. The purpose of the silicon oxide layer  
159 is to protect the unexposed silicon area during an etching process. Triangular prism arrays were  
160 photo-lithographically patterned on a 1- $\mu\text{m}$ -thick layer of photoresist (PR), HPR 504, on top of the  
161 silicon dioxide layer. The pattern consists of repetitive rectangular lines with a uniform width and  
162 a gap of 1.5  $\mu\text{m}$  between each line. Patterns for different line widths were considered in fabrication  
163 varying from 8-13  $\mu\text{m}$  to study the cooling performance of different triangular sizes. The silicon  
164 dioxide layer was etched using an advanced oxide etching (AOE) process that etches only the  
165 exposed photoresist layer until the silicon surface is exposed. The photoresist layer was solely  
166 required for leaving the pattern on the silicon dioxide layer and therefore, after etching of the  
167 silicon dioxide layer, it was completely stripped by  $\text{O}_2$  plasma treatment. Before the silicon etching  
168 process started, the silicon wafer was treated with hydrofluoric acid again for complete removal  
169 of native oxide on the exposed silicon surface which might hinder the process of silicon etching.  
170 The silicon wafer was then immersed into a tetramethylammonium hydroxide (TMAH) solution  
171 (25 wt. %), a silicon etchant, at temperature of 90 °C and only the unprotected silicon area was  
172 etched. TMAH etches silicon leaving V-grooves and the angle between the sidewalls and the (100)  
173 plane is 54.7 °. Anisotropic etching property of TMAH achieves triangular prism arrays on the  
174 silicon wafer. Typical etch rate of TMAH for the (100) plane was 1.0  $\mu\text{m}/\text{min}$  and for the (110)  
175 plane was 1.4  $\mu\text{m}/\text{min}$  at 90 °C [48]. The etching time was carefully controlled based on the widely  
176 known etching rate of silicon. Silicon dioxide layer was perfectly removed by buffered oxide etch



177 (BOE) solution, mixture of 6:1 (v/v)  $\text{NH}_4\text{F}:\text{HF}$ , and the mold for the triangular prism array  
178 structure was completed. Totally, three molds for different triangular size parameter of 8, 9, and  
179  $10\ \mu\text{m}$  were fabricated. The patterned surface of the silicon mold was sputtered with 320 nm of  
180 chromium which acts as a PDMS anti-adhesion layer. PDMS and its curing agent were mixed  
181 together in the mass ratio of 10:1 then spin-coated with  $20\ \mu\text{m}$  thickness on a  $525\ \mu\text{m}$  thick  $4\ \text{cm}$   
182  $\times 4\ \text{cm}$  glass substrate with 160 nm thick silver sputtered at the back. On top of the spin-coated  
183 PDMS, the silicon mold facing patterned surface toward PDMS was pressed gently and cured in  
184 an oven at  $80\ ^\circ\text{C}$  for 4 hrs. After the curing process finished, the patterned silicon mold was gently  
185 removed, achieving a three layered passive radiative cooler sample consisting of a triangular prism  
186 array structured PDMS, glass and silver at the bottom. **The fabrication process is elaborated more**  
187 **in Fig. S1 in the Supplementary Materials.**

188

### 189 **3. Theory/calculation**

190 To carry out the cooling performance analysis numerically for the fabricated bio-inspired cooler  
191 such as the net cooling power and achieved temperature reduction below the temperature of  
192 ambient air, the energy balance state of the daytime passive radiative cooling was carefully  
193 investigated. The net radiative cooling power,  $P_{cool}$ , is shown below [11]:

194

$$195 \quad P_{cool} = P_{rad}(T_{prc}) - P_{atm}(T_{atm}) - P_{sun} - P_{con}(T_{prc}, T_{atm}), \quad (1)$$

196

197 where  $P_{rad}$  is the thermally radiated power of the cooling device [W],  $T_{prc}$  is the surface  
198 temperature of the cooler [K],  $P_{atm}$  is the power absorbed by the passive radiative cooler from the  
199 ambient atmosphere [W],  $T_{atm}$  is the ambient atmosphere temperature [K],  $P_{sun}$  is the absorbed

200 power by the surface of the cooler from the incident solar irradiance [W], and  $P_{con}$  is the convective  
 201 and conductive power gained by the cooler surface [W]. The radiative thermal energy emitted from  
 202 the cooler at the cooler temperature,  $T_{prc}$ , is given by:

$$204 \quad P_{rad}(T_{prc}) = A_{prc} \int d\Omega \cos\theta \int_0^\infty d\lambda I_{BB}(T_{prc}, \lambda) \varepsilon(\lambda), \quad (2)$$

203  
 206 where  $A_{prc}$  is the area of the sky facing cooler [m<sup>2</sup>].  $I_{BB}(T, \lambda) = \frac{2hc^2}{\lambda^5} \frac{1}{e^{hc/(\lambda k_B T)} - 1}$  is the  
 207 spectral distribution of the thermal energy radiated by a black-body [W/(m<sup>3</sup>sr)] at any temperature  
 208  $T$  and  $h$  is Planck's constant of  $6.63 \times 10^{-34}$  J·s,  $c$  is the universal physical constant for speed of light  
 209 which is  $3.00 \times 10^8$  m/s,  $\lambda$  is wavelength [m], and  $k_B$  is denoted as the Boltzmann constant of  
 210  $1.38 \times 10^{-23}$  J/K,  $\varepsilon(\lambda)$  refers to the emissivity spectra (0.25- 25  $\mu$ m) of the radiative cooling devices  
 211 and the measured emission spectrum of the coolers used.  $P_{atm}(T_{atm})$  is the absorbed power by the  
 212 cooler surface from the thermal radiation emitted from the surrounding atmosphere at the  
 213 temperature of  $T_{atm}$  and can be defined as:

$$215 \quad P_{atm}(T_{atm}) = A_{prc} \int d\Omega \cos\theta \int_0^\infty d\lambda I_{BB}(T_{atm}, \lambda) \varepsilon(\lambda) \varepsilon_{atm}(\lambda), \quad (3)$$

214  
 217 where  $\varepsilon_{atm}(\lambda)$  is the emission spectrum (0.25-25  $\mu$ m) of the atmosphere [49]. Validation of the  
 218 numerical model was carried out by comparing the numerically estimated cooling power with  
 219 previous studies [11–15, 33] by using the widely known atmospheric transmittance data measured  
 220 in Mauna Kea located in Hawaii, U.S.A. with conditions of 1.5 air mass and precipitable water  
 221 vapor of 1.0 mm [50]. Thermal energy is emitted from the surrounding atmosphere and absorbed  
 222 by the radiative cooler with the ratio of its emissivity degrading net cooling performance. The law

223 of Kirchhoff's radiation clearly states that the material's absorptivity and emissivity can be  
224 considered equal because under a thermodynamic equilibrium state, the fraction of an emissive  
225 power from a perfect black-body shows it to be equivalent to its ratio of the incoming power to the  
226 absorbed power of the object [2–10].

227

$$228 \quad P_{sun} = A_{prc} \int_0^{\infty} d\lambda I_{AM1.5}(\lambda) \varepsilon(\lambda), \quad (4)$$

229

230 is the absorbed power by the radiative cooler from incoming solar irradiance.  $I_{AM1.5}$  is the **AM**  
231 **1.5 G** spectrum which can be defined by the solar intensity of densely populated regions which are  
232 located at moderate altitude [51] and used widely in the photovoltaic industry [52].  $P_{con}$  is the  
233 parasitic heat delivered to the cooler from the surrounding atmosphere by conduction and  
234 convection and can be defined as:

235

$$236 \quad P_{con}(T_{prc}, T_{atm}) = A_{prc} h_{con} (T_{atm} - T_{prc}), \quad (5)$$

237

238 where  $h_{con}$  is the heat transfer coefficient for the heat transfer between the cooler and the  
239 surrounding atmosphere due to conduction and convection [W/(m<sup>2</sup>K)].

240

## 241 **4. Results and Discussion**

### 242 **4.1. FDTD optimizations**

243 The emission spectra were investigated for three different geometrical configurations of the  
244 PDMS thermal emitter with various characteristic lengths of the proposed geometries. These  
245 configurations are conventional uniform flat surfaces, ordinary hair resembling periodic circular

246 arrays, and lastly, Saharan silver ant hair inspired periodic triangular arrays. The optical property  
247 comparison in different geometrical structures is to show that the triangular prism shape adopted  
248 surface can enhance MIR emissivity of the conventional flat emitter. The PDMS emitter with  
249 circular arrays which represents commonly recognized hair was also studied to further investigate  
250 the uniqueness of the triangular hair structure compared to the ordinary hair structure. Referring  
251 to Fig. 1c, characteristic lengths ( $a$ ) of the geometries were selected as the thickness of the uniform  
252 flat surface, the diameter of the circle, and the bottom length of the triangle. The triangular  
253 structure was set to isosceles triangle with equal angle of  $54.7^\circ$  because the angle is limited to that  
254 for the wet etching process on a silicon wafer. Knowing that Mie scattering occurs when incoming  
255 wavelength and object share similar size, characteristic lengths of the proposed structure were  
256 selected within the range of 2-15  $\mu\text{m}$  to investigate MIR emissivity enhancement of the emitter  
257 caused by the scattering effect. Fig. 1c shows the averaged MIR emissivity of three different  
258 geometries along the characteristic lengths. This plot represents the PDMS emitter with triangular  
259 arrays on the surface, always achieving a stronger thermal emission property than the other two  
260 geometrical configurations. Furthermore, when the size parameter of the triangle was between 8-  
261  $13\mu\text{m}$ , the simulated average emissivity within the atmospheric transparent window showed a  
262 higher value than when the size was outside this range. This is mainly due to the triangular prism  
263 structure with a size between 8-13  $\mu\text{m}$  that can provide a gradual change in the refractive index in  
264 8-13  $\mu\text{m}$  between air and PDMS. Impedance mismatch occurring between air and PDMS can be  
265 reduced, enhancing the overall emissivity of PDMS. Different size of triangular prism PDMS  
266 gradient index layer within the size parameter of 8-13  $\mu\text{m}$  shows varying influence on emissivity  
267 within this bandwidth due to the difference in resonance points. The size parameter of 8  $\mu\text{m}$  which  
268 is four times larger than the original hair showed the strongest improvement in thermal emission

269 within 8-13  $\mu\text{m}$ , resulting in an average emissivity value of 0.98. Fig. 1d shows the emission  
270 spectra for three different configurations sharing the same characteristic length of 8  $\mu\text{m}$  in the  
271 wavelength range of 8-13  $\mu\text{m}$ . At the same characteristic length, the triangular PDMS emitter  
272 clearly shows the highest MIR emissivity over the other two emitters. Referring to the FDTD  
273 simulation study, triangular structure is the best for enhancing thermal emission within MIR and  
274 the triangle with optimized characteristic length of 8  $\mu\text{m}$  induces the most Mie scattering within  
275 8-13  $\mu\text{m}$ , resulting in the highest average emissivity of 0.98 within 8-13  $\mu\text{m}$ .

276

#### 277 **4.2. Optical measurement and numerical analysis**

278 Based on the simulation study, a PDMS-SiO<sub>2</sub>-Ag three layered cooler, in which the PDMS  
279 thermal emitter (4-inch wafer) shown in Fig. 2a was of an optimized triangular geometry with a  
280 characteristic length of 8  $\mu\text{m}$ , was micro-fabricated. Silicon molds with triangular arrays shown in  
281 Fig. 2b were used to print patterns on the PDMS surface. Fig. 2c shows the enlarged cross-section  
282 of the silicon mold. Validation of the simulation results was followed by investigating PDMS  
283 emitters with different characteristic lengths of the triangle, 8  $\mu\text{m}$ , 9  $\mu\text{m}$  and 10  $\mu\text{m}$ , together with  
284 a uniform 100  $\mu\text{m}$  thick PDMS emitter. To investigate the overall cooling performance  
285 improvement of the bio-inspired cooler compared to the previously proposed radiative coolers  
286 [15], the uniform 100  $\mu\text{m}$  thick PDMS emitter was chosen rather than a uniform PDMS emitter  
287 with a similar characteristic length of triangular patterned PDMS emitter. To compare and  
288 understand the optical properties of the samples, the emissivity of the samples over the ultraviolet  
289 (UV) to IR wavelength ranges shown in Fig. 3a were measured by an UV/VIS/NIR spectrometer  
290 and Fourier transform infrared spectroscopy (FTIR). Fig. 3b shows the emissivity spectrum in the  
291 UV to NIR region of the coolers with PDMS in uniform and triangular structures with size

292 parameters at 8, 9, and 10  $\mu\text{m}$ . Solar radiation absorbed by the coolers can be numerically  
293 calculated by the multiplication of the measured absorptivity of coolers within UV-NIR and AM  
294 1.5 G solar irradiance at unit wavelength. All four different samples of radiative coolers showed  
295 low solar absorption power density about 20-25  $\text{W}/\text{m}^2$  that mainly absorbed within the ultraviolet  
296 spectrum. The triangular prism structure did not show any improvement in solar reflection but  
297 mainly enhanced the thermal radiation of the passive radiative cooler. Fig. 3c shows the emissivity  
298 spectra of the four different coolers in the wavelength range of 8–13  $\mu\text{m}$ . The average emissivity  
299 for the uniform PDMS cooler was 0.92 and the triangular PDMS cooler with a size parameter of  
300 8  $\mu\text{m}$  showed 0.98, an enhancement of 6.5%. The triangular PDMS cooler with a size parameter  
301 of 10  $\mu\text{m}$  showed the lowest emissivity (0.93) among the patterned PDMS coolers, indicating the  
302 triangular structure to have better emission performance within the 8-13  $\mu\text{m}$  spectrum range than  
303 the uniform PDMS cooler. Lastly, a comparison solar reflectivity and MIR emission spectrum of  
304 the previously reported daytime passive radiative coolers [11, 13-15, 53, 54] with the triangular  
305 patterned PDMS cooler was conducted to understand the performance improvement. Fig. 4a shows  
306 that the bio-inspired triangular PDMS cooler is not really outstanding in solar reflectance among  
307 all the radiative coolers previously studied. Due to the wide usage of silver as a reflector in the  
308 daytime passive radiative coolers, most coolers including the bio-inspired triangular PDMS cooler  
309 (i.e. this work) show high solar reflection (i.e. at least 97%). The highest solar reflection was  
310 achieved by the PTFE-Ag cooler which can reflect 99% of incoming solar irradiance, absorbing  
311 only  $\sim 10 \text{ W}/\text{m}^2$ , which is  $15 \text{ W}/\text{m}^2$  less than the bio-inspired triangular PDMS cooler (i.e. this  
312 study) [53]. However, Fig. 4b shows that the bio-inspired triangular PDMS cooler shows very  
313 clear difference in MIR emissivity by having almost unity spectrum in the 8-13  $\mu\text{m}$  wavelength.  
314 This obvious distinction shows the developed radiative cooler has almost achieved the maximum

315 **emission performance for the daytime passive radiative cooling technique.** The prismatic structure  
316 obviously showed superiority in MIR emissivity compared to the uniform surface and with the  
317 measured optical characteristics, the cooling performance improvement can be investigated  
318 numerically.

319

320 To validate the result analyzed by the energy balance equation, the cooling performance of a  
321 fabricated uniform 100  $\mu\text{m}$  thick PDMS silica-mirror was analyzed based on its measured optical  
322 properties and compared with the previously reported value [15]. When there are no parasitic heat  
323 gains from the ambient atmosphere (i.e.  $h_{con} = 0 \text{ W}/(\text{m}^2\text{K})$ ), Fig. 5a shows that the fabricated  
324 uniform 100  $\mu\text{m}$  PDMS cooler can passively provide a net cooling power of  $127 \text{ W}/\text{m}^2$  at the  
325 temperature of the surrounding atmosphere,  $T_{atm}$ , of  $27 \text{ }^\circ\text{C}$  that perfectly matches with the  
326 previously reported net cooling power of the uniform 100  $\mu\text{m}$  thick PDMS silica-mirror [15]. The  
327 patterned PDMS cooler can provide the maximum net cooling power of  $144 \text{ W}/\text{m}^2$  at the ambient  
328 air temperature of  $27 \text{ }^\circ\text{C}$  which corresponds to an enhancement of 13.4 % compared to uniform  
329 PDMS cooler. The ideal passive radiative emitter, perfect solar reflection in the spectrum of  $0.3 -$   
330  $2.5 \mu\text{m}$  and perfect emission in the spectrum of  $8 - 13 \mu\text{m}$ , was estimated to provide a maximum  
331 net radiative cooling power of  $132 \text{ W}/\text{m}^2$  at the ambient air temperature of  $27 \text{ }^\circ\text{C}$  [55]. However,  
332 the cooling performance can be further enhanced by exploiting spectrum regions outside the  
333 atmospheric transparent window,  $2.5 - 8 \mu\text{m}$  and  $13 - 25 \mu\text{m}$ . Utilizing this broad spectrum region,  
334  $2.5 - 25 \mu\text{m}$ , an ideal radiative cooler with perfect solar reflection in the spectrum of  $0.3 - 2.5 \mu\text{m}$   
335 and perfect emission in the spectrum of  $2.5 - 25 \mu\text{m}$  can produce  $207 \text{ W}/\text{m}^2$  maximum cooling  
336 power at the ambient of  $27 \text{ }^\circ\text{C}$  [55]. The total thermal radiation absorbed from the atmosphere to  
337 the cooler is increased but the outgoing thermal emission from the cooler exceeds the incoming

338 radiation, thereby enhancing the net cooling performance. The triangular structure greatly  
339 enhances emissivity within 8 - 13  $\mu\text{m}$  and outside the main atmospheric transparent window,  
340 ultimately exceeding the cooling power of the narrow-band ideal radiative cooler. Fig. 5b presents  
341 an estimated cooling power of the cooler at a condition where the ambient,  $T_{atm}$ , is 27 °C and a  
342 parasitic heat coefficient of  $h_{con} = 10 \text{ W}/(\text{m}^2\text{K})$  [15]. In Fig. 5b, temperature of the cooler is  
343 reduced below the ambient air temperature by 8.7 °C for the uniform 100  $\mu\text{m}$  PDMS cooler. The  
344 patterned PDMS cooler can decrease the surface temperature by a maximum of 9.8 °C which  
345 shows the triangular structure greatly enhances the cooling performance compared to the uniform  
346 PDMS cooler.

347

### 348 **4.3. Field investigation**

349 To validate the numerically estimated cooling performance and study the actual cooling behavior  
350 in non-ideal atmospheric conditions, 24-hour field investigations were conducted under the sky  
351 condition of Hong Kong. The radiative cooling performance investigation was performed on the  
352 building roof top where the cooler can perfectly face the sky. In the experiment setup, minimizing  
353 the parasitic heat gains to the coolers was the top priority in order to maximize the net cooling  
354 power. The experiment site was perfectly covered by a calcium-magnesium silicate thermal  
355 insulation sheet to minimize the conductive heat generated from the concrete surface heated from  
356 the sunlight. Petri dishes with three acrylic legs which can minimize the contact surface with the  
357 ground were placed on top of the sheet. The fabricated coolers were placed in the Petri dishes to  
358 limit the thermal contact with the ambient air. Additional acrylic supporting structures were also  
359 fabricated to minimize the contact with the Petri dishes. Finally, to minimize the convective heat  
360 transfer by wind, the Petri dishes were covered by a very thin polyethylene film which is



361 transparent within the wavelength ranges of solar radiation and passive radiative cooling. A  
362 detailed schematic design of the experimental setup can be found in Fig. 6a. Fig. 6b shows the  
363 experimental setup on the rooftop of a building. A data acquisition device, National Instruments  
364 NI 9213, was used to record (frequency: 1 s, accuracy:  $\pm 0.02$  °C) the temperatures of coolers and  
365 ambient air measured by thermocouples. Thermocouples used in the field investigations were  
366 calibrated to eliminate measurement error and directly attached to the back side of the cooler  
367 having the silver layer. The experiment was conducted during clear days of June and September.

368

369 Totally, 2 different samples were prepared to carry out the comparative study. These consisted  
370 of a uniform 100  $\mu\text{m}$  PDMS-SiO<sub>2</sub>-Ag cooler and an 8  $\mu\text{m}$  triangular patterned PDMS-SiO<sub>2</sub>-Ag  
371 cooler that showed the highest net cooling power among all the patterned coolers with different  
372 sizes of triangle. Fig. 7a presents the four different temperature profiles of the 8  $\mu\text{m}$  triangular and  
373 the 100  $\mu\text{m}$  thick uniform PDMS-SiO<sub>2</sub>-Ag coolers with and without solar shade for a 48 hr cycle  
374 measurement in Hong Kong (Date: Sep-30-2018 to Sep-31-2018). The average relative humidity  
375 of these two days was 87 % and the sky was very clear with 0-1 oktas. Under the humid Hong  
376 Kong weather, no matter shaded or unshaded, during the night time, both the triangular patterned  
377 and the uniform cooler showed cooling effects with a temperature reduction of 6.1 °C and 5.2 °C  
378 below the ambient air temperature, respectively. The triangular patterned PDMS cooler showed a  
379 lower surface temperature by average 1 °C than the uniform PDMS cooler. The uniform PDMS  
380 cooler was reported to have a temperature decrease of 8.4 °C during night time of Pasadena,  
381 California [15]. The lower value of the measured temperature reduction below the ambient during  
382 the night time is due to the high relative humidity in Hong Kong. The transparency of the  
383 atmospheric window that lies in 8-13  $\mu\text{m}$  spectrum is closely affected by the vapor concentration

384 in the atmosphere that results in low transparency, i.e., high absorption of atmosphere is due to the  
385 high relative humidity and this limits the escape of the thermal radiation to the cold universe. The  
386 MIR absorption of atmosphere enhanced by three-folds as the precipitable water vapor increases  
387 from 1.5 cm to 6 cm [3], showing the limitation of the passive radiative cooling in humid weather.  
388 Conditions of low humidity and cloudless sky can result in strong transmittance in the MIR  
389 spectrum facilitating the radiative cooler to produce the ideal cooling performance. However, the  
390 field investigation showed that the triangular pattern could enhance the radiative cooling effect,  
391 reducing the temperature nearly 1 °C more than the uniform PDMS cooler. Fig. 7b (i.e. a zoom-in  
392 figure) shows the four different temperature profiles of the 8 μm triangular and the 100 μm thick  
393 uniform PDMS-SiO<sub>2</sub>-Ag coolers under shaded and unshaded conditions during the peak daytime  
394 of Hong Kong (Date: Sep-31-2018). During the daytime, even under the clear sky, 0-1 oktas, it is  
395 clear that both coolers without shading were unable to produce a cooling effect. At the peak  
396 daytime, both the triangular PDMS cooler and the uniform PDMS cooler without shading was  
397 measured with a temperature higher than the ambient air temperature by 5.1 °C and 6.0 °C,  
398 respectively. Due to the characteristics of the tropical climate, both coolers, without shading, were  
399 unable to deliver cooling performance under the peak solar irradiation as incident solar energy  
400 exceeded the radiated thermal energy from the coolers to the atmospheric transparency window.  
401 However, even in this poor weather condition for radiative cooling, the triangular structured cooler  
402 could maintain a temperature 1 °C below the temperature of the uniform cooler. In order to provide  
403 cooling during the peak of Hong Kong's daytime, solar shades, fabricated by aluminum sheet,  
404 were installed to shade the coolers during daytime to minimize the incident solar energy delivered  
405 to the coolers. With the solar shades partially blocking the incoming sunlight, at the peak daytime,  
406 daytime cooling was achieved with the maximum temperature reduction (average temperature

407 difference between 12:00 – 13:00 (Date: 31-Sep-2018)) of 6.2 °C and 5.1 °C below the ambient  
408 for the triangular and uniform, respectively.

409

410 Net radiative cooling power measurement of both a uniform 100  $\mu\text{m}$  PDMS-SiO<sub>2</sub>-Ag cooler and  
411 an 8  $\mu\text{m}$  triangular patterned PDMS-SiO<sub>2</sub>-Ag cooler was conducted in a humid climate condition  
412 of Hong Kong. Silicon heating mats with a heating capacity of 20 W were attached at the back of  
413 both coolers. The cooling power produced by the radiative cooler will be equal to the heating  
414 power from the heater when its temperature remains the same as the ambient air temperature. Thus,  
415 electrical current flow delivered to the cooling power measurement system was controlled by a  
416 feedback loop to maintain the temperature of the cooler equal to the ambient. The net cooling  
417 power of these two coolers was estimated by summing up electrical energy consumed by the heater  
418 pad in an hourly rate. Fig. 7c presents the collected data for temperature and net cooling power of  
419 the uniform 100  $\mu\text{m}$  PDMS-SiO<sub>2</sub>-Ag cooler and the 8  $\mu\text{m}$  triangular patterned PDMS-SiO<sub>2</sub>-Ag  
420 cooler. The peak ambient air temperature during the daytime was measured near 33 °C at 2 pm  
421 (08-June-2019), when 19.7 W/m<sup>2</sup> cooling power was recorded for the triangular patterned PDMS  
422 cooler, while a net cooling power of 17.9 W/m<sup>2</sup> was obtained from the uniform PDMS cooler.  
423 During nighttime operation, the lowest temperature of ambient air was measured at 19 °C (5 am,  
424 08-June-2019) and the triangular patterned PDMS cooler produced 14.3 W/m<sup>2</sup> cooling power,  
425 while 13.3 W/m<sup>2</sup> cooling power was recorded for the uniform PDMS cooler. Lower temperature  
426 of ambient at night weakened the thermal radiation emitted from both coolers resulting in lower  
427 nocturnal cooling power compared to the daytime cooling. In total, both patterned and non-  
428 patterned radiative coolers showed weakened cooling performance compared to the outcome

429 achieved in the clear and dry climatic conditions. Nevertheless, the triangular patterned PDMS  
430 cooler showed a 10% enhanced net cooling power than that of the uniform PDMS cooler.

431  
432 Table 1 summarizes the recent achievements in daytime passive radiative cooling regarding their  
433 structural designs, optical properties including solar reflectance and MIR emissivity, and cooling  
434 performance. Uniform flat PDMS radiative cooler demonstrated experimentally the highest  
435 daytime cooling performance by generating  $127 \text{ W/m}^2$  [15]. Optimized  $\text{TiO}_2\text{-SiO}_2$  alternating  
436 multi-layered cooler theoretically predicted a higher net cooling power of  $136.6 \text{ W/m}^2$  while its  
437 field investigation demonstrated only  $14.3 \text{ W/m}^2$  due to the poor sky condition of sub-tropical  
438 Hong Kong [13]. The bio-inspired radiative cooler in this work presents the highest cooling  
439 performance numerically, showing the net cooling power of  $144 \text{ W/m}^2$ . However, due to  
440 unfavorable sky condition of low atmospheric transparency, its field investigation result shows a  
441 net cooling power of  $19.7 \text{ W/m}^2$  and temperature reduction of  $6.2 \text{ }^\circ\text{C}$  under direct sunlight. While  
442 a majority of the work was conducted under ideal sky conditions, it should be noted that daytime  
443 passive radiative cooling is mostly needed in hot sub-tropical or tropical regions. Its cooling  
444 performance deteriorates significantly in high humid weather conditions, but by minimizing  
445 incoming solar irradiance, daytime cooling effect can be successfully achieved.

446

## 447 5. Conclusion

448 In conclusion, the bio-inspired thermal selective surface utilizing the unique triangular structure  
449 of the Saharan silver ant hair was fabricated by nano-imprinting. Triangular prismatic hair  
450 originally functioned to mainly enhance solar reflection, but was unable to meet the required solar  
451 reflection for daytime passive cooling. Its application approach in designing a cooler was set to

452 enhance MIR emissivity by utilizing gradient refractive index change provided by the triangular  
453 structure. For the first time, we have demonstrated geometrical modification on a polymeric  
454 surface to enhance the emission property. The geometrical details of the triangle and the overall  
455 design of the cooler were optimized through the FDTD simulation, proposing a passive radiative  
456 cooler design with PDMS triangular arrays at a size characteristic of 8  $\mu\text{m}$ , four times larger than  
457 the original hair of the Saharan silver ant, deposited on the silver coated silica wafer. Mathematical  
458 analysis on temperature reduction and cooling performance based on optical measurement were  
459 conducted to validate the simulation work, proving that the bio-inspired triangular structure can  
460 greatly enhance the emissivity within 8-13  $\mu\text{m}$  at the maximum of 0.98, exceeding the cooling  
461 performance of existing intricate nanophotonic surfaces. Theoretically, the triangular pattern can  
462 enhance the net cooling power to 144  $\text{W}/\text{m}^2$  which is the highest value among the developed  
463 daytime passive radiative coolers. Also, experimentally, the field investigation on cooling  
464 performance of the triangular PDMS cooler was studied in Hong Kong to understand its  
465 practicality in a humid weather climate. With the poor atmospheric transparency of Hong Kong's  
466 tropical climate, an average atmospheric transmittance within 8-13  $\mu\text{m}$  below 0.5, daytime cooling  
467 effect could be achieved using solar shades, and the surface temperature could be sustained at a  
468 maximum 6.2  $^{\circ}\text{C}$  below the ambient which corresponds to a net cooling power of 19.7  $\text{W}/\text{m}^2$  in a  
469 non-vacuumed condition. This investigation delivers a significant meaning by demonstrating the  
470 unprecedented daytime passive radiative cooling in a humid climate condition, exceeding the  
471 cooling performance of leading coolers which are already available. Overall, applications of  
472 triangular prism structure can greatly improve the cooling performance of a plain uniform surface  
473 and can be further applied to different surfaces to optimize the desired optical properties. Further  
474 modification to the triangular structure can be conducted to maximize the reflection of solar

475 irradiance to achieve a stronger passive cooling system. Our study facilitates application of passive  
476 radiative cooling as a zero-energy input sustainable system to high energy consuming areas such  
477 as indoor space cooling [39-41], photovoltaic industry [37, 38], personal thermal managing and  
478 regulating system [35, 36].

Table 1. Summary of structural design, optical properties and cooling performance of daytime passive radiative coolers.

Authors	Structural Designs	Methodology	Solar Reflectance	MIR Emissivity	Experimental Locations & Conditions	Temperature Reduction (°C)	Cooling Power (W/m <sup>2</sup> )
Bao et al. [56]	2 layers of TiO <sub>2</sub> , SiO <sub>2</sub> , and SiC nanoparticles	Numerical and Field Investigation	0.907	0.90	Shanghai, China	5	25
					Non-vacuum		
Chen et al. [14]	3 layers of 70 nm thick Si <sub>3</sub> N <sub>4</sub> , 700 μm thick Si, and 150 nm thick Al solar reflector at the back.	Numerical and Field Investigation	0.967	0.56	Stanford, California, USA	42	60
					Vacuum		
Jeong et al. [13]	8 alternating layers of 500 nm thick TiO <sub>2</sub> and 500 nm thick SiO <sub>2</sub> layers with 200 nm thick Ag solar reflector and supported by 750 μm Si layer at the back.	Numerical and Field Investigation	0.942	0.84	Hong Kong, China	7.2	14.3
					Non-vacuum		
Kecebas et al. [54]	Top 9 layers consisting of alternating TiO <sub>2</sub> , SiO <sub>2</sub> , and Al <sub>2</sub> O <sub>3</sub> each 200 nm thick. Lower 4 layers consisting of alternating TiO <sub>2</sub> and SiO <sub>2</sub> , each 20 nm thick. 50 nm thick Ag solar reflector at the back.	Numerical	0.960	0.69	N.A.	N.A.	103

Kecebas et al. [54]	Top 9 layers consisting of alternating TiO <sub>2</sub> and SiO <sub>2</sub> , each 200 nm thick. Below 4 layers consisting of alternating TiO <sub>2</sub> and SiO <sub>2</sub> , each 60 nm thick. 50 nm thick Ag solar reflector at the back.	Numerical	0.965	0.54	N.A.	N.A.	85.8
Kou et al. [15]	3 layers of 100 μm thick PDMS, 500 μm thick SiO <sub>2</sub> , and 120 nm thick Ag solar reflector at the back	Numerical and Field Investigation	0.975	0.92	Pasadena, California, USA	8.2	127
					Non-vacuum		
Raman et al. [11]	7 alternating layers of 230 nm thick SiO <sub>2</sub> , 485 nm thick HfO <sub>2</sub> , 688 nm thick SiO <sub>2</sub> , 13 nm thick HfO <sub>2</sub> , 73 nm thick SiO <sub>2</sub> , 34 nm thick HfO <sub>2</sub> , and 54 nm thick SiO <sub>2</sub> with 200 nm thick Ag solar reflector and supported by 750 μm Si layer at the back	Numerical and Field Investigation	0.970	0.65	Stanford, California, USA	4.9	40.1
					Non-vacuum		
Zhai et al. [33]	Micrometer-sized SiO <sub>2</sub> spheres randomly distributed in a matrix material of polymethylpentene (TPX)	Numerical and Field Investigation	0.969	0.93	Cave creek, Arizona, USA	N.A.	93
					Non-vacuum		



This work	3 layers of 8 $\mu\text{m}$ thick triangular prism patterned PDMS, 500 $\mu\text{m}$ thick $\text{SiO}_2$ , and 120 nm thick Ag solar reflector at the back	Numerical and Field Investigation	0.975	0.98	Hong Kong, China	6.2	19.7
					Non-vacuum		

480

481 **Conflict of Interest**

482 The authors declare that there is no conflict of interest.

483

484 **Acknowledgments**

485 The funding for this research is provided by the Hong Kong Research Grant Council via  
486 Collaborative Research Fund (CRF) account C6022-16G and General Research Fund (GRF)  
487 account 16200518, and also the City University of Hong Kong StartUp Fund via the account code  
488 of 9610411. We also acknowledge Nanosystem Fabrication Facility (NFF) of HKUST for the  
489 device/system fabrication.

490

491 **References**

- 492 [1] S. Catalanotti, V. Cuomo, G. Piro, D. Ruggi, V. Silvestrini, G. Troise, The radiative cooling of  
493 selective surfaces, *Solar Energy*. 17.2 (1975) 83-89. doi:10.1016/0038-092x(75)90062-6.
- 494 [2] C.G. Granqvist, A. Hjortsberg, Surfaces for radiative cooling: Silicon monoxide films on  
495 aluminum, *Applied Physics Letters*. 36 (1980) 139–141. doi:10.1063/1.91406.
- 496 [3] C.G. Granqvist, A. Hjortsberg, Radiative cooling to low temperatures: General considerations  
497 and application to selectively emitting SiO films, *Journal of Applied Physics*. 52 (1981) 4205–  
498 4220. doi:10.1063/1.329270.
- 499 [4] A. Harrison, M. Walton, Radiative cooling of TiO<sub>2</sub> white paint, *Solar Energy*. 20 (1978) 185–  
500 188. doi:10.1016/0038-092x(78)90195-0.
- 501 [5] P. Berdahl, M. Martin, F. Sakkal, Thermal performance of radiative cooling panels,  
502 *International Journal of Heat and Mass Transfer*. 26 (1983) 871–880. doi:10.1016/s0017-  
503 9310(83)80111-2.

- 504 [6] P. Berdahl, Radiative cooling with MgO and/or LiF layers, *Applied Optics*. 23 (1984) 370-372.  
505 doi:10.1364/ao.23.000370.
- 506 [7] T.M. Nilsson, G.A. Niklasson, C.G. Granqvist, A solar reflecting material for radiative cooling  
507 applications: ZnS pigmented polyethylene, *Solar Energy Materials and Solar Cells*. 28 (1992)  
508 175–193. doi:10.1016/0927-0248(92)90010-m.
- 509 [8] T.M. Nilsson, G.A. Niklasson, Radiative cooling during the day: simulations and experiments  
510 on pigmented polyethylene cover foils, *Solar Energy Materials and Solar Cells*. 37 (1995) 93–  
511 118. doi:10.1016/0927-0248(94)00200-2.
- 512 [9] P. Berdahl, Comments on radiative cooling efficiency of white pigmented paints, *Solar Energy*.  
513 54 (1995) 203. doi:10.1016/0038-092x(95)90031-a.
- 514 [10] C.N. Suryawanshi, C.-T. Lin, Radiative Cooling: Lattice Quantization and Surface Emissivity  
515 in Thin Coatings, *ACS Applied Materials & Interfaces*. 1 (2009) 1334–1338.  
516 doi:10.1021/am900200r.
- 517 [11] A.P. Raman, M.A. Anoma, L. Zhu, E. Rephaeli, S. Fan, Passive radiative cooling below  
518 ambient air temperature under direct sunlight, *Nature*. 515 (2014) 540–544.  
519 doi:10.1038/nature13883.
- 520 [12] C. Tso, K. Chan, C.Y. Chao, A field investigation of passive radiative cooling under Hong  
521 Kong’s climate, *Renewable Energy*. 106 (2017) 52–61. doi:10.1016/j.renene.2017.01.01.
- 522 [13] S.Y. Jeong, C.Y. Tso, J. Ha, Y.M. Wong, C.Y. Chao, B. Huang, et al., Field investigation of  
523 a photonic multi-layered TiO<sub>2</sub> passive radiative cooler in sub-tropical climate, *Renewable*  
524 *Energy*. 146 (2020) 44–55. doi:10.1016/j.renene.2019.06.119.

- 525 [14] Z. Chen, L. Zhu, A. Raman, S. Fan, Radiative cooling to deep sub-freezing temperatures  
526 through a 24-h day–night cycle, *Nature Communications*. 7 (2016).  
527 doi:10.1038/ncomms13729.
- 528 [15] J.-L. Kou, Z. Jurado, Z. Chen, S. Fan, A.J. Minnich, Daytime Radiative Cooling Using Near-  
529 Black Infrared Emitters, *ACS Photonics*. 4 (2017) 626–630.  
530 doi:10.1021/acsp Photonics.6b00991.
- 531 [16] S.-Y. Lin, J.G. Fleming, E. Chow, J. Bur, K.K. Choi, A. Goldberg, Enhancement and  
532 suppression of thermal emission by a three-dimensional photonic crystal, *Physical Review B*.  
533 62 (2000). doi:10.1103/physrevb.62.r2243.
- 534 [17] A. Narayanaswamy, G. Chen, Thermal emission control with one-dimensional  
535 metallodielectric photonic crystals, *Physical Review B*. 70 (2004).  
536 doi:10.1103/physrevb.70.125101.
- 537 [18] I. Celanovic, D. Perreault, J. Kassakian, Resonant-cavity enhanced thermal emission, *Physical*  
538 *Review B*. 72 (2005). doi:10.1103/physrevb.72.075127.
- 539 [19] E. Rephaeli, S. Fan, Absorber and emitter for solar thermo-photovoltaic systems to achieve  
540 efficiency exceeding the Shockley-Queisser limit, *Optics Express*. 17 (2009) 15145-15159.  
541 doi:10.1364/oe.17.015145.
- 542 [20] J.L. Gall, M. Olivier, J.-J. Greffet, Experimental and theoretical study of reflection and  
543 coherent thermal emission by a SiC grating supporting a surface-phonon polariton, *Physical*  
544 *Review B*. 55 (1997) 10105–10114. doi:10.1103/physrevb.55.10105.
- 545 [21] J.B. Pendry, Radiative exchange of heat between nanostructures, *Journal of Physics:*  
546 *Condensed Matter*. 11 (1999) 6621–6633. doi:10.1088/0953-8984/11/35/301.

- 547 [22] C. Luo, A. Narayanaswamy, G. Chen, J.D. Joannopoulos, Thermal Radiation from Photonic  
548 Crystals: A Direct Calculation, *Physical Review Letters*. 93 (2004).  
549 doi:10.1103/physrevlett.93.213905.
- 550 [23] D.L.C. Chan, M. Soljačić, J.D. Joannopoulos, Thermal emission and design in one-  
551 dimensional periodic metallic photonic crystal slabs, *Physical Review E*. 74 (2006).  
552 doi:10.1103/physreve.74.016609.
- 553 [24] D.L.C. Chan, M. Soljačić, J.D. Joannopoulos, Thermal emission and design in 2D-periodic  
554 metallic photonic crystal slabs, *Optics Express*. 14 (2006) 8785-8796.  
555 doi:10.1364/oe.14.008785.
- 556 [25] J.G. Fleming, S.Y. Lin, I. El-Kady, R. Biswas, K.M. Ho, All-metallic three-dimensional  
557 photonic crystals with a large infrared bandgap, *Nature*. 417 (2002) 52–55.  
558 doi:10.1038/417052a.
- 559 [26] E. Rephaeli, S. Fan, Tungsten black absorber for solar light with wide angular operation range,  
560 *Applied Physics Letters*. 92 (2008) 211107. doi:10.1063/1.2936997.
- 561 [27] K.A. Arpin, M.D. Losego, P.V. Braun, Electrodeposited 3D Tungsten Photonic Crystals with  
562 Enhanced Thermal Stability, *Chemistry of Materials*. 23 (2011) 4783–4788.  
563 doi:10.1021/cm2019789.
- 564 [28] M. Wang, C. Hu, M. Pu, C. Huang, Z. Zhao, Q. Feng, et al., Truncated spherical voids for  
565 nearly omnidirectional optical absorption, *Optics Express*. 19 (2011) 20642-20649.  
566 doi:10.1364/oe.19.020642.
- 567 [29] S. Zhang, Y. Li, G. Feng, B. Zhu, S. Xiao, L. Zhou, et al., Strong infrared absorber: surface-  
568 microstructured Au film replicated from black silicon, *Optics Express*. 19 (2011) 20462-  
569 20467. doi:10.1364/oe.19.020462.

- 570 [30] M.M. Hossain, B. Jia, M. Gu, *Metamaterials: A Metamaterial Emitter for Highly Efficient*  
571 *Radiative Cooling (Advanced Optical Materials 8/2015)*, *Advanced Optical Materials*. 3  
572 (2015) 980–980. doi:10.1002/adom.201570046.
- 573 [31] C. Zou, G. Ren, M.M. Hossain, S. Nirantar, W. Withayachumnankul, T. Ahmed, et al., *Metal-*  
574 *Loaded Dielectric Resonator Metasurfaces for Radiative Cooling*, *Advanced Optical*  
575 *Materials*. 5 (2017) 1700460. doi:10.1002/adom.201700460.
- 576 [32] K. Hwang, Y.-S. Jung, Y.-J. Heo, F.H. Scholes, S.E. Watkins, J. Subbiah, et al., *Toward Large*  
577 *Scale Roll-to-Roll Production of Fully Printed Perovskite Solar Cells*, *Advanced Materials*.  
578 27 (2015) 1241–1247. doi:10.1002/adma.201404598.
- 579 [33] Y. Zhai, Y. Ma, S.N. David, D. Zhao, R. Lou, G. Tan, et al., *Scalable-manufactured*  
580 *randomized glass-polymer hybrid metamaterial for daytime radiative cooling*, *Science*. 355  
581 (2017) 1062–1066. doi:10.1126/science.aai7899.
- 582 [34] A.R. Gentle, G.B. Smith, *Radiative Heat Pumping from the Earth Using Surface Phonon*  
583 *Resonant Nanoparticles*, *Nano Letters*. 10 (2010) 373–379. doi:10.1021/nl903271d.
- 584 [35] P.-C. Hsu, X. Liu, C. Liu, X. Xie, H.R. Lee, A.J. Welch, et al., *Personal Thermal Management*  
585 *by Metallic Nanowire-Coated Textile*, *Nano Letters*. 15 (2014) 365–371.  
586 doi:10.1021/nl5036572.
- 587 [36] J.K. Tong, X. Huang, S.V. Boriskina, J. Loomis, Y. Xu, G. Chen, *Infrared-Transparent*  
588 *Visible-Opaque Fabrics for Wearable Personal Thermal Management*, *ACS Photonics*. 2  
589 (2015) 769–778. doi:10.1021/acsphotonics.5b00140.
- 590 [37] L. Zhu, A. Raman, K.X. Wang, M.A. Anoma, S. Fan, *Radiative cooling of solar cells*, *Optica*.  
591 1 (2014) 32-38. doi:10.1364/optica.1.000032.

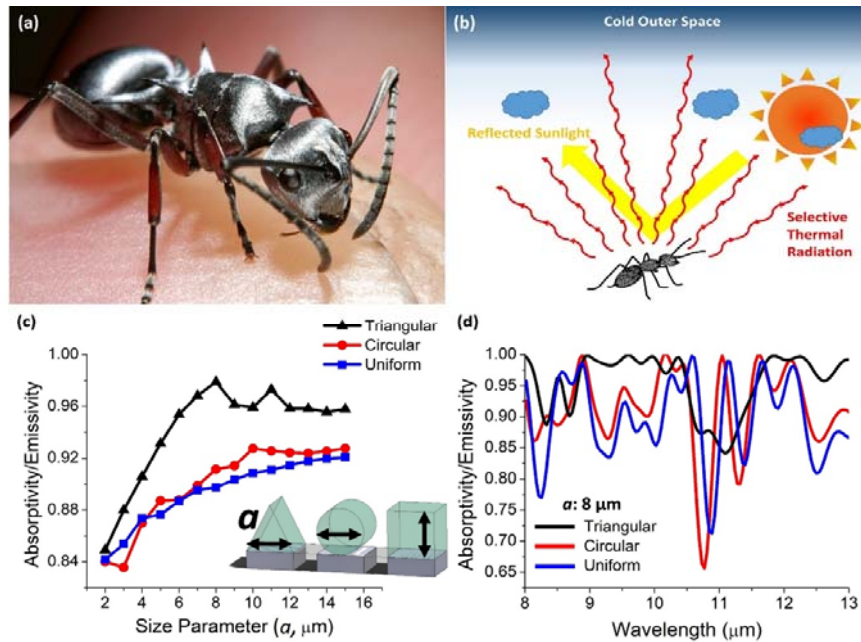
- 592 [38] W. Li, Y. Shi, K. Chen, L. Zhu, S. Fan, Passive cooling of solar cells with a comprehensive  
593 photonic approach, 2017 IEEE 60th International Midwest Symposium on Circuits and  
594 Systems (MWSCAS). (2017). doi:10.1109/mwscas.2017.8053056.
- 595 [39] E.A. Goldstein, A.P. Raman, S. Fan, Sub-ambient non-evaporative fluid cooling with the sky,  
596 *Nature Energy*. 2 (2017). doi:10.1038/nenergy.2017.143.
- 597 [40] W. Wang, N. Fernandez, S. Katipamula, K. Alvine, Performance assessment of a photonic  
598 radiative cooling system for office buildings, *Renewable Energy*. 118 (2018) 265–277.  
599 doi:10.1016/j.renene.2017.10.062.
- 600 [41] S.Y. Jeong, C.Y. Tso, M. Zouagui, Y.M. Wong, C.Y.H. Chao, A numerical study of daytime  
601 passive radiative coolers for space cooling in buildings, *Building Simulation*. 11 (2018) 1011–  
602 1028. doi:10.1007/s12273-018-0474-4.
- 603 [42] C. Paquet, E. Kumacheva, Nanostructured polymers for photonics, *Materials Today*. 11 (2008)  
604 48–56. doi:10.1016/s1369-7021(08)70056-7.
- 605 [43] R. Wehner, A.C. Marsh, S. Wehner, Desert ants on a thermal tightrope, *Nature*. 357 (1992)  
606 586–587. doi:10.1038/357586a0.
- 607 [44] N.N. Shi, C.-C. Tsai, F. Camino, G.D. Bernard, N. Yu, R. Wehner, Keeping cool: Enhanced  
608 optical reflection and radiative heat dissipation in Saharan silver ants, *Science*. 349 (2015)  
609 298–301. doi:10.1126/science.aab3564.
- 610 [45] Q. Willot, P. Simonis, J.-P. Vigneron, S. Aron, Total Internal Reflection Accounts for the  
611 Bright Color of the Saharan Silver Ant, *Plos One*. 11 (2016).  
612 doi:10.1371/journal.pone.0152325.
- 613 [46] C.F. Bohren, D.R. Huffman, Absorption and scattering of light by small particles, Wiley-  
614 VCH, Weinheim, 2009.

- 615 [47] A. Srinivasan, B. Czapla, J. Mayo, A. Narayanaswamy, Infrared dielectric function of  
616 polydimethylsiloxane and selective emission behavior, *Applied Physics Letters*. 109 (2016)  
617 061905. doi:10.1063/1.4961051.
- 618 [48] O. Tabata, R. Asahi, H. Funabashi, K. Shimaoka, S. Sugiyama, Anisotropic etching of silicon  
619 in TMAH solutions, *Sensors and Actuators A: Physical*. 34 (1992) 51–57. doi:10.1016/0924-  
620 4247(92)80139-t.
- 621 [49] A. Berk, G.P. Anderson, P.K. Acharya, L.S. Bernstein, L. Muratov, J. Lee, et al.,  
622 MODTRAN5: 2006 update, *Algorithms and Technologies for Multispectral, Hyperspectral,  
623 and Ultraspectral Imagery XII*. (2006). doi:10.1117/12.665077.
- 624 [50] S.D. Lord, *A new software tool for computing earth's atmospheric transmission of near- and  
625 far-infrared radiation*, Ames Research Center, Moffett Field, CA, 1992.
- 626 [51] C. Gueymard, D. Myers, K. Emery, Proposed reference irradiance spectra for solar energy  
627 systems testing, *Solar Energy*. 73 (2002) 443-467. Doi:10.1016/s0038-092x(03)00005-7
- 628 [52] *Tables for Reference Solar Spectral Irradiances: Direct Normal and Hemispherical on 37  
629 Tilted Surface*, (n.d.). doi:10.1520/g0173.
- 630 [53] P. Yang, C. Chen, Z.M. Zhang, *A dual-layer structure with record-high solar reflectance for  
631 daytime radiative cooling*, *Solar Energy*. 169 (2018) 316–324.  
632 doi:10.1016/j.solener.2018.04.031.
- 633 [54] M.A. Kecebas, M.P. Menguc, A. Kosar, K. Sendur, *Passive radiative cooling design with  
634 broadband optical thin-film filters*, *Journal of Quantitative Spectroscopy and Radiative  
635 Transfer*. 198 (2017) 179–186. doi:10.1016/j.jqsrt.2017.03.046.



- 636 [55] Z. Huang, X. Ruan, Nanoparticle embedded double-layer coating for daytime radiative  
637 cooling, *International Journal of Heat and Mass Transfer*. 104 (2017) 890–896.  
638 doi:10.1016/j.ijheatmasstransfer.2016.08.009.
- 639 [56] H. Bao, C. Yan, B. Wang, X. Fang, C. Zhao, X. Ruan, Double-layer nanoparticle-based  
640 coatings for efficient terrestrial radiative cooling, *Solar Energy Materials and Solar Cells*. 168  
641 (2017) 78–84. doi:10.1016/j.solmat.2017.04.020.

# 1 Figure Captions



2

3 Fig. 1. (a) Photograph of Saharan silver ant, *Cataglyphis bombycina* (b) A schematic diagram

4 of thermoregulatory effect discovered in the Saharan silver ant (c) FDTD simulation

5 result for averaged MIR emissivity (8-13  $\mu\text{m}$ ) of three different geometrical

6 configurations (triangular prism arrays (black solid line), circular rod arrays (red solid

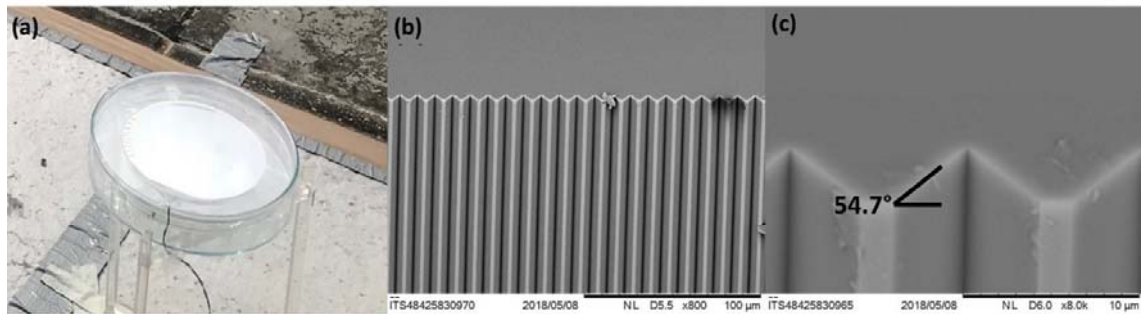
7 line), and uniform flat layer (blue solid line)) along with characteristic length of 2-15

8  $\mu\text{m}$  (d) FDTD simulation result for MIR emission spectrum (8-13  $\mu\text{m}$ ) of emitters with

9 triangular prism arrays (black solid line), circular rod arrays (red solid line), and

10 uniform flat layer (blue solid line) at a constant characteristic length of 8  $\mu\text{m}$

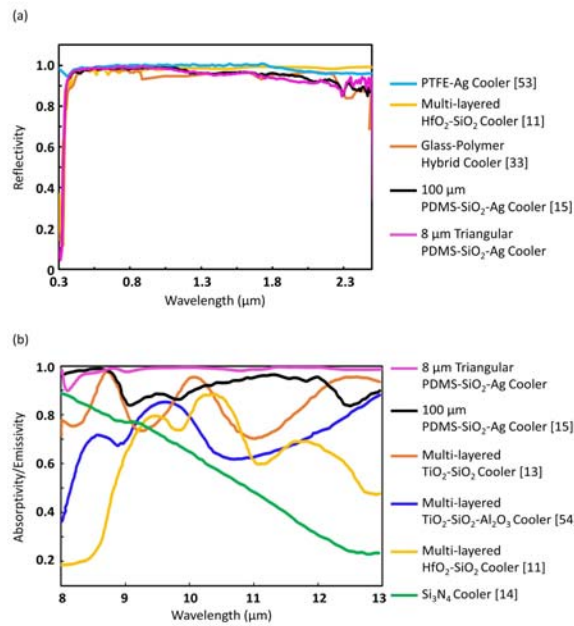
11



13

14 Fig. 2. (a) A fabricated 4-inch wafer size 8 μm characteristic length triangular PDMS-SiO<sub>2</sub>-Ag  
15 daytime passive radiative cooler under direct sunlight. (b) SEM image of the fabricated  
16 silicon mold with 8 μm characteristic length triangular arrays with a scale bar at 100  
17 μm. (c) SEM image of the fabricated silicon mold with 8 μm characteristic length  
18 triangular arrays with a scale bar at 10 μm.

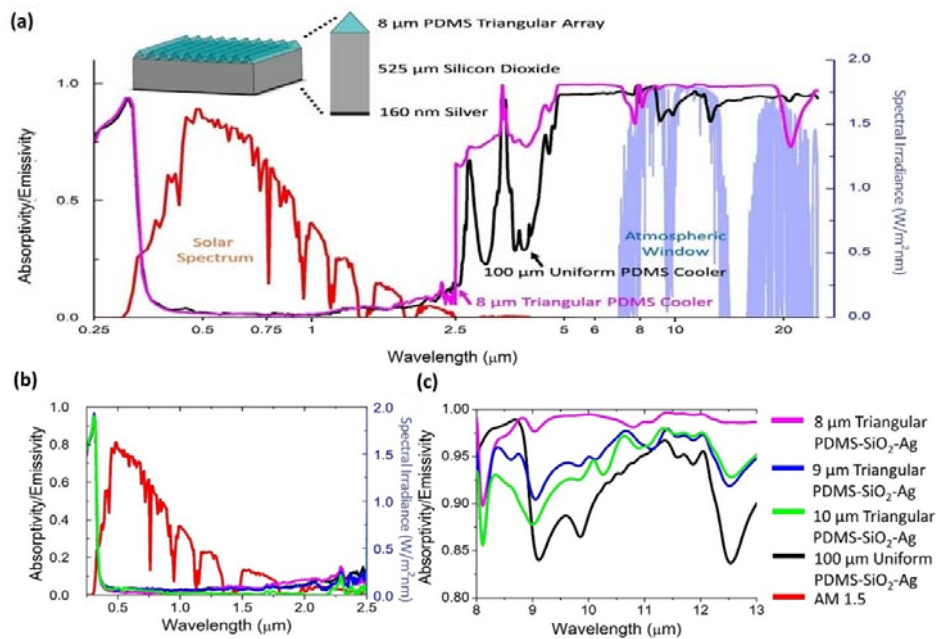
19



21

22 Fig. 3. (a) Measured full emission spectrum of the uniform 100 μm thick PDMS-SiO<sub>2</sub>-Ag  
 23 (black solid line) and the patterned PDMS-SiO<sub>2</sub>-Ag with triangular prism array of a  
 24 size parameter at 8 μm (pink solid line) in the wavelength range of 0.25-25 μm. (b)  
 25 Measured emissivity of the uniform 100 μm thick PDMS-SiO<sub>2</sub>-Ag (black solid line),  
 26 the patterned PDMS-SiO<sub>2</sub>-Ag with triangular prism array of a size parameter at 8 μm  
 27 (pink solid line), a size parameter at 9 μm (blue solid line), a size parameter at 10 μm  
 28 (green solid line) in the wavelength range of 0.25-2.5 μm. The AM 1.5 solar spectrum  
 29 (red solid line). (c) Measured emissivity of the uniform 100 μm thick PDMS-SiO<sub>2</sub>-Ag  
 30 (black solid line), the patterned PDMS-SiO<sub>2</sub>-Ag with triangular prism arrays of a size  
 31 parameter at 8 μm (pink solid line), a size parameter at 9 μm (blue solid line), a size  
 32 parameter at 10 μm (green solid line) in the wavelength range of 8-13 μm.

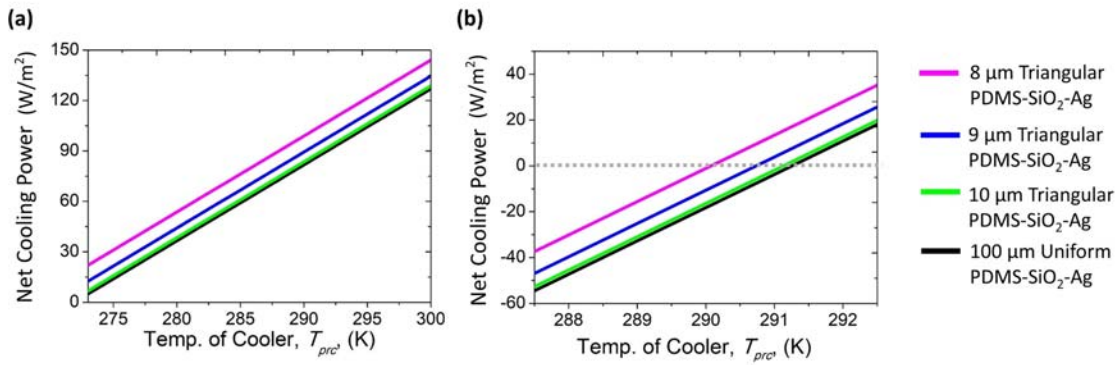
33



35

36 Fig. 4. (a) Reflectivity spectrum within 0.3-2.5  $\mu\text{m}$  of PTFE-Ag cooler [53] (light blue solid  
 37 line),  $\text{HfO}_2\text{-SiO}_2$  alternating multi-layered radiative cooler [11] (yellow solid line),  
 38 glass-polymer hybrid cooler [33] (orange solid line), 100  $\mu\text{m}$  uniform PDMS polymer  
 39 based radiative cooler [15] (black solid line), and 8  $\mu\text{m}$  triangular PDMS polymer based  
 40 radiative cooler (pink solid line, this work) (b) Emission spectrum within 8-13  $\mu\text{m}$  of 8  
 41  $\mu\text{m}$  triangular PDMS polymer based radiative cooler (pink solid line, this work), 100  
 42  $\mu\text{m}$  uniform PDMS polymer based radiative cooler [15] (black solid line),  $\text{TiO}_2\text{-SiO}_2$   
 43 alternating multi-layered radiative cooler [13] (orange solid line),  $\text{TiO}_2\text{-SiO}_2\text{-Al}_2\text{O}_3$   
 44 alternating multi-layered radiative cooler [54] (blue solid line),  $\text{HfO}_2\text{-SiO}_2$  alternating  
 45 multi-layered radiative cooler [11] (yellow solid line), and  $\text{Si}_3\text{N}_4$  based radiative cooler  
 46 [14] (green solid line).

47



48

49

50 Fig. 5. (a) Numerically estimated cooling power of the uniform 100 μm thick PDMS-SiO₂-Ag

51 (black solid line), the patterned PDMS-SiO₂-Ag with triangular prism arrays of a size  
52 parameter at 8 μm (pink solid line), a size parameter at 9 μm (blue solid line), a size

53 parameter at 10 μm (green solid line) with changing cooler temperature at a heat gain

54 condition of  $h_{con} = 0 \text{ W}/(\text{m}^2\text{K})$ . (b) Numerically estimated cooling power of the

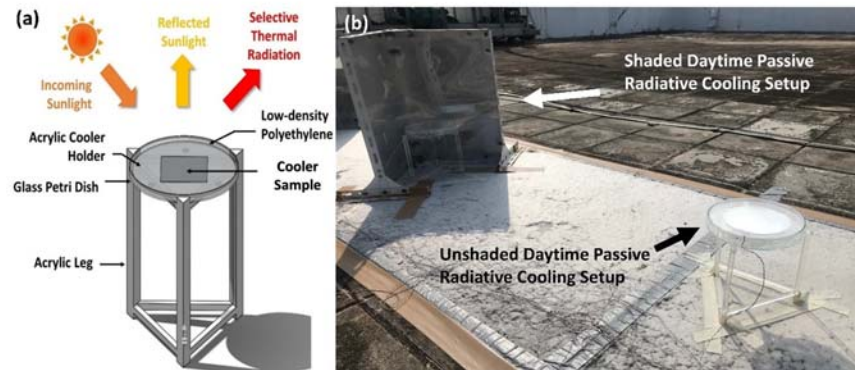
55 uniform 100 μm thick PDMS-silica-mirror (black solid line), the patterned PDMS-

56 SiO₂-Ag with triangular prism arrays of a size parameter at 8 μm (pink solid line), a

57 size parameter at 9 μm (blue solid line), a size parameter at 10 μm (green solid line)

58 with changing cooler temperature at a heat gain condition of  $h_{con} = 10 \text{ W}/(\text{m}^2\text{K})$ .

59



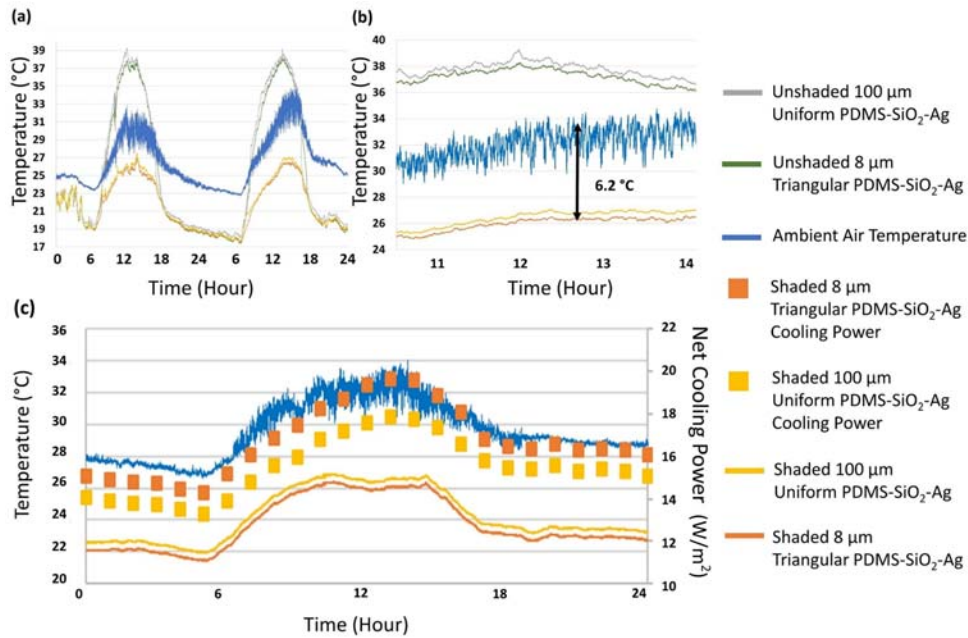
60

61

62 Fig. 6. (a) A schematic diagram of experimental setup for daytime passive radiative cooling (b)

63 Experimental setups for both shaded and unshaded daytime passive radiative cooling.

64



65

66

67 Fig. 7. (a) Temperature profile of the unshaded uniform 100  $\mu\text{m}$  thick PDMS-SiO<sub>2</sub>-Ag (grey

68 solid line), the unshaded 8  $\mu\text{m}$  triangle PDMS-SiO<sub>2</sub>-Ag (green solid line), and the

69 temperature of ambient (blue solid line), the shaded uniform 100  $\mu\text{m}$  thick PDMS-SiO<sub>2</sub>-

70 Ag (yellow solid line), the shaded 8  $\mu\text{m}$  PDMS-SiO<sub>2</sub>-Ag (orange), through a 48 hrs

71 cycle (Date: 30-Sep-2018 to 31-Sep-2018). The average daytime relative humidity was

72 87 % and 0-1 oktas sky condition was observed. The average global solar intensity was

73 measured to be 1010 W/m<sup>2</sup> at peak daytime (11:00 am to 13:00 pm). (b) Zoom-in of the

74 temperature profile (Date: 31-Sep-2018) with the device under direct solar irradiation.

75 The shaded 8  $\mu\text{m}$  triangle PDMS-SiO<sub>2</sub>-Ag cooler (orange solid line) achieved a

76 temperature 6.2 °C below the temperature of ambient. (c) Net cooling power (square

77 box) and temperature (line) profiles of the shaded 100  $\mu\text{m}$  uniform PDMS-SiO<sub>2</sub>-Ag

78 cooler (yellow) and the shaded 8  $\mu\text{m}$  triangular patterned PDMS-SiO<sub>2</sub>-Ag cooler

79 (orange) at the ambient air temperature (blue) during a 24-hr cycle (Date: 08-June-

80 2019). The average relative humidity during the daytime and nighttime was 85 % and

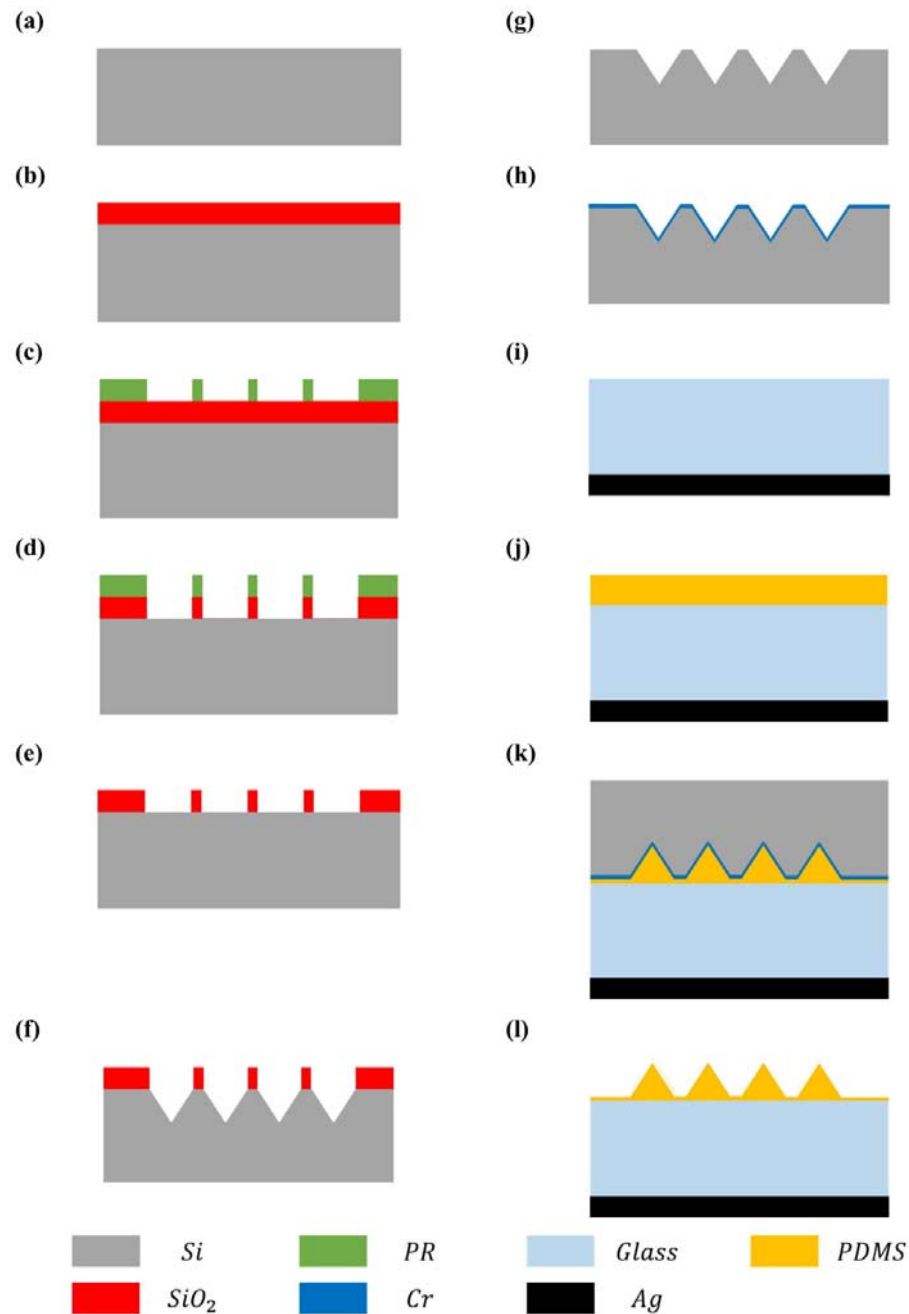
81 65 %, respectively. 0-1 oktas sky condition was observed. The average global solar



82 intensity was measured at  $1020 \text{ W/m}^2$  during the peak daytime (from 12:00 pm to 2:00  
83 pm).

84

## 1 Supplementary Materials



2

3 Fig. S1. Fabrication process flow of the bio-inspired passive radiative cooler. (a) Preparation  
 4 of a 525  $\mu\text{m}$  thick P-type 4-inch silicon wafer cleaned by Piranha and hydrofluoric acid  
 5 solution. (b) Thermal oxidation of the silicon wafer for 60 nm. (c) Photo-lithography of the  
 6 pattern on the silicon wafer. (d) AOE process to etch the thermal oxide layer for 30 s. (e) Photo  
 7 resist layer strip off process. (f) Silicon wet etching process with TMAH solution (g) BOE

- 8 process to remove the remaining thermal oxide layer. (h) Sputter 160 nm thickness chromium
- 9 on the surface of the mold. (i) Sputter 160 nm Silver at the back of the silicon dioxide substrate.
- 10 (j) Spin-coat 20  $\mu\text{m}$  PDMS on the silicon dioxide substrate. (k) Nano-imprint process (l)
- 11 Removal of the mold after baking.
- 12